Received: 30 November 2020 | Revised: 31 March 2021 | Accepted: 19 April 2021

DOI: 10.1002/humu.24211

RESEARCH ARTICLE

Human Mutation HGVS HUMAN GENOME VARIATION SOCIETY WILEY

New cases that expand the genotypic and phenotypic spectrum of Congenital NAD Deficiency Disorder

Justin O. Szot[1] | Anne Slavotinek[2] | Karen Chong[3] | Oliver Brandau[4] | Marjan Nezarati[5,6] | Anna M. Cueto-González[7] | Millan S. Patel[8] | Walter P. Devine[9] | Shannon Rego[2] | Alicia P. Acyinena[2] | Patrick Shannon[10] | Diane Myles-Reid[3] | Susan Blaser[11] | Tim V. Mieghem[12] | Halenur Yavuz-Kienle[4] | Heyko Skladny[4] | Kristen Miller[5] | Miereia D. T. Riera[13] | Silvia A. Martínez[14] | Eduardo F. Tizzano[7,15] | Lucie Dupuis[16] | Dimitri James Stavropoulos[17] | Vanda McNiven[16] | Roberto Mendoza-Londono[16] | Alison M. Elliott[8] | The CAUSES Study | Robert S. Phillips[18,19] | Gavin Chapman[1,20] | Sally L. Dunwoodie[1,20,21]

[1]Victor Chang Cardiac Research Institute, Sydney, New South Wales, Australia

[2]Department of Pediatrics, University of California San Francisco, San Francisco, California, USA

[3]Prenatal Diagnosis and Medical Genetics Program, Department of Obstetrics and Gynecology, Mount Sinai Hospital, Toronto, Ontario, Canada

[4]SYNLAB MVZ Humangenetik Mannheim, Mannheim, Germany

[5]Genetics Program, North York General Hospital, Toronto, Ontario, Canada

[6]Department of Paediatrics, University of Toronto, Toronto, Ontario, Canada

[7]Department of Clinical and Molecular Genetics, Vall d'Hebron Barcelona Hospital Campus, Barcelona, Spain

[8]Department of Medical Genetics, University of British Columbia, Vancouver, British Columbia, Canada

[9]Department of Anatomic Pathology, University of California, San Francisco, California, USA

[10]Pathology and Laboratory Medicine, Mount Sinai Hospital, Toronto, Ontario, Canada

[11]The Hospital for Sick Children, Toronto, Ontario, Canada

[12]Fetal Medicine Program, Department of Obstetrics and Gynecology, Mount Sinai Hospital, Toronto, Ontario, Canada

[13]Metabolic Unit and Pediatric Neurology Department, Vall d'Hebron Barcelona Hospital Campus, Barcelona, Spain

[14]Fetal Medicine Unit and Obstetrics Department, Vall d'Hebron Barcelona Hospital Campus, Barcelona, Spain

[15]Medicine Genetics Group, Vall d'Hebron Research Institute, Vall d'Hebron Barcelona Hospital Campus, Autonomous University of Barcelona, Barcelona, Spain

[16]Department of Pediatrics, Division of Clinical and Metabolic Genetics, The Hospital for Sick Children, University of Toronto, Toronto, Ontario, Canada

[17]Genome Diagnostics, Department of Paediatric Laboratory Medicine, The Hospital for Sick Children, Toronto, Ontario, Canada

[18]Department of Biochemistry and Molecular Biology, University of Georgia, Athens, Georgia, USA

[19]Department of Chemistry, University of Georgia, Athens, Georgia, USA

[20]Faculty of Medicine, University of New South Wales, Sydney, New South Wales, Australia

[21]Faculty of Science, University of New South Wales, Sydney, New South Wales, Australia

Correspondence: Sally L. Dunwoodie, Victor Chang Cardiac Research Institute, Lowy Packer, Bldg, 405 Liverpool St., Darlinghurst, Sydney, NSW 2010, Australia.
Email: s.dunwoodie@victorchang.edu.au

Funding information

The Key Foundation; University of Toronto McLaughlin Centre; Office of Health and Medical Research of the New South Wales Government; National Health and Medical Research Council Project Grant, Grant/Award Number: 1162878; National Health and Medical Research Council Fellowship, Grant/Award Number: 1042002; National Human Genome Research Institute, Grant/Award Number: U01HG009599

Abstract

Nicotinamide adenine dinucleotide (NAD) is an essential coenzyme involved in over 400 cellular reactions. During embryogenesis, mammals synthesize NAD *de novo* from dietary L-tryptophan via the kynurenine pathway. Biallelic, inactivating variants in three genes encoding enzymes of this biosynthesis pathway (*KYNU*, *HAAO*, and *NADSYN1*) disrupt NAD synthesis and have been identified in patients with multiple malformations of the heart, kidney, vertebrae, and limbs; these patients have Congenital NAD Deficiency Disorder *HAAO* and four families with biallelic variants in *KYNU*. These patients present similarly with multiple malformations of the heart, kidney, vertebrae, and limbs, of variable severity. We show that each variant identified in these patients results in loss-of-function, revealed by a significant reduction in NAD levels via yeast genetic complementation assays. For the first time, missense mutations are identified as a cause of malformation and shown to disrupt enzyme function. These missense and frameshift variants cause moderate to severe NAD deficiency in yeast, analogous to insufficient synthesized NAD in patients. We hereby expand the genotypic and corresponding phenotypic spectrum of Congenital NAD Deficiency Disorder.

KEYWORDS

Congenital NAD Deficiency Disorder, *de novo* NAD biosynthesis, *HAAO*, *KYNU*, kynurenine pathway, NAD, nicotinamide adenine dinucleotide

1 | INTRODUCTION

Nicotinamide adenine dinucleotide (NAD) is an essential coenzyme with roles in almost all key biological processes (Ansari & Raghava, 2010) and known redox functions in over 400 cellular reactions (Rajman et al., 2018). NAD metabolism fluctuates widely between tissues and subcellular compartments with a half-life ranging from 15 min to 15 h (Liu et al., 2018). Owing to an inability to import NAD, mammalian cells synthesize NAD *de novo* from L-tryptophan via the kynurenine pathway, or from the conversion of its dietary precursors nicotinamide, nicotinic acid, and nicotinamide riboside via the Preiss-Handler and salvage pathways (Cambronne & Kraus, 2020). NAD is largely consumed by sirtuins, cyclic ADP-ribose synthases, and poly(ADP-ribose) polymerases with essential functions in metabolism, DNA repair, circadian rhythm, immunity, injury and stress response, and epigenetics. Although NAD dynamics in health and disease are well-studied in adults (Katsyuba et al., 2020; Rajman et al., 2018), comparatively little is known regarding the necessity for NAD during embryogenesis.

Congenital NAD Deficiency Disorder is characterized by birth defects in humans most commonly involving the heart, kidney, vertebrae, and limbs, and stemming from an insufficient synthesis of NAD *de novo* during embryogenesis. To date, causes are limited to biallelic loss-of-function (LOF) variants in *HAAO* or *KYNU* (Shi et al., 2017), and LOF or reduced function variants in *NADSYN1* (Szot et al., 2020). All three genes encode nonredundant enzymes of the *de novo* NAD biosynthesis pathway whose inactivation manifests downstream NAD deficiency in affected individuals. Although there is significant phenotypic variability, individuals with biallelic *NADSYN1* variants predicting LOF exhibit the most severe defects incompatible with life (Szot et al., 2020), likely owing to an inability to synthesize NAD from nicotinic acid via the Preiss-Handler pathway, unlike those with *HAAO* or *KYNU* variants. In contrast, some patients with biallelic *HAAO* or *KYNU* LOF variants are surviving (Shi et al., 2017).

KYNU encodes the pyridoxal-5′-phosphate (PLP; vitamin B6)-dependent kynureninase. Within the *de novo* NAD biosynthesis pathway, kynureninase cleaves L-3-hydroxykynurenine to produce 3-hydroxyanthranilic acid (Phillips, 2011). KYNU is a homodimer with the PLP-binding site at the monomer-monomer interface. KYNU can also catalyze the conversion of L-kynurenine to anthranilic acid, but about 250-fold more slowly. This preference for 3-hydroxy-L-kynurenine results from the Asn333 residue, which donates a hydrogen bond to the phosphate group of PLP and accepts a hydrogen bond from the 3-hydroxyl group of the substrate in the active site (Lima et al., 2007). To date, only two patients have been reported with disease-causal *KYNU* variants; both with biallelic LOF variants that lack enzyme activity and manifest downstream NAD deficiency (Shi et al., 2017). It is likely that pathogenic variants, other than protein truncation, impairing the catalytic site may similarly impact

protein function and, by extension, reduce total synthesized NAD via the *de novo* biosynthesis pathway.

HAAO encodes the nonheme iron-dependent enzyme 3-hydroxyanthranilate 3,4-dioxygenase. Within the *de novo* NAD biosynthesis pathway, HAAO functions immediately after KYNU and cleaves the benzene ring of substrate 3-hydroxyanthranilic acid, in the presence of oxygen and ferrous iron (Fe^{2+}), producing an unstable intermediate 2-amino-3-carboxymuconic acid semialdehyde, which spontaneously rearranges into quinolinic acid. To date, only two patients have been reported with disease-causal *HAAO* variants; both with biallelic LOF variants that lack enzyme activity and manifest downstream NAD deficiency (Shi et al., 2017). Similar to KYNU, it is likely that variants impairing the catalytic site or activity overall reduce total downstream NAD synthesized via the *de novo* biosynthesis pathway.

Here, we have identified seven unrelated patients harboring biallelic *HAAO* or *KYNU* variants and show through yeast genetic complementation studies that each yeast mutant results in reduced NAD levels that are likely due to impaired *de novo* NAD biosynthesis.

2 | METHODS

2.1 | Editorial policies and ethical considerations

Informed consent was obtained for all individuals sequenced in this study. The *HAAO* and *KYNU* variants reported in this manuscript are accessible in ClinVar with the submission number SUB8498741.

2.2 | Clinical information

Extended clinical descriptions and family histories are presented in the Supporting Information.

2.3 | DNA sequencing and analysis

Trio exome or genome sequencing was performed for all patients and parents using DNA isolated from amniotic fluid, fetal tissue, or whole blood. Variant calling, alignment, and interpretation were then either performed in-house per patient or via GeneDx. Detailed sequencing and analysis methodologies per patient are presented in the Supporting Information.

2.4 | Cloning of yeast expression constructs

pDONR201 HAAO was generated as described (Szot et al., 2020). Variants c.128G>A p.(Arg43Lys), c.141C>A p.(His47Gln), c.43del p.(Arg15Glyfs*99), c.301G>T p.(Gly101Trp), and c.323G>A p.(Arg108Gln) were introduced into pDONR201 HAAO cDNA by site-directed mutagenesis with primers listed in Table S1. *HAAO* wild-type and mutant cDNA inserts were then transferred to pAG416GPD (Addgene plasmid #14148) by Gateway LR reaction. Human *KYNU* cDNA was amplified from Origene:RC214932 using cloning primers (Table S1), then gateway cloned into pDONR201 via BP reaction (Thermo Fisher Scientific) according to the manufacturer's instructions. Variants c.788A>G p.(His263Arg), c.616G>A p.(Glu206Lys), c.361_363del p.(Lys121del), c.1035T>A p.(Ser345-Arg), c.489del p.(Ala164Profs*26), c.1282C>T p.(Arg428Trp), c.592A>G p.(Thr198Ala), and c.170-1G>T p.(Val57Glufs*21) were introduced into pDONR201 KYNU via site-directed mutagenesis with primers listed in Table S1. Finally, *KYNU* wild-type and mutant cDNA inserts were then transferred to pAG416GPD by Gateway LR reaction. All introduced variants were confirmed by Sanger sequencing.

2.5 | Yeast BY4741/BY4742 *Δbna1* and BY4741/BY4742 *Δbna5* generation and transformations

Diploid *Saccharomyces cerevisiae* BY4741/BY4742 (*MATa/MATα his3Δ1/his3Δ1 leu2Δ0/leu2Δ0 ura3Δ0/ura3Δ0 met15Δ0 lys2Δ0*) with homozygous deletion of the yeast orthologs of human *HAAO* or *KYNU* (*bna1* or *bna5*, respectively) were sourced from the EUROpean *Saccharomyces Cerevisiae* ARchive for Functional Analysis (Winzeler et al., 1999) via I. Dawes, R. Stocker, and A. Ayer (Australia).

Yeast transformations were performed using a Yeast Transformation Kit (Sigma-Aldrich) according to the manufacturer's instructions. Transformed yeast was transferred onto agar plates (20 g/L Agar bacteriological (Agar No. 1; Oxoid), 20 g/L *D*-(+)-glucose (Sigma-Aldrich), 1.7 g/L Yeast Nitrogen Base, without amino acids, without ammonium sulfate (AMRESCO); 5 g/L ammonium sulfate (Sigma-Aldrich), amino acids (Sigma-Aldrich): 260 mg/L leucine, 76 mg/L isoleucine, 120 mg/L valine, 46 mg/L histidine, 90 mg/L tryptophan, 55 mg/L adenine). Positive transformants were genotyped for correct plasmid uptake via direct polymerase chain reaction (PCR) from yeast cultures (Amberg et al., 2006) and Sanger sequencing.

2.6 | Enzymatic NAD^+/NADH assays

Δbna1 HAAO, p.(Arg43Lys), p.(His47Gln), p.(Arg15Glyfs*99), p.(Gly101Trp), p.(Arg108Gln), and KYNU yeast were grown in a shaker at 30°C for 24 h in "plus-niacin" media (20 g/L *D*-(+)-glucose (Sigma-Aldrich), 1.7 g/L Yeast Nitrogen Base, without amino acids, without ammonium sulfate (AMRESCO); 5 g/L ammonium sulfate (Sigma-Aldrich), amino acids (Sigma-Aldrich): 260 mg/L leucine, 76 mg/L isoleucine, 120 mg/L valine, 46 mg/L histidine, 90 mg/L tryptophan, 55 mg/L adenine). Yeast was washed, resuspended in "minus-niacin media" (20 g/L *D*-(+)-glucose (Sigma-Aldrich), 6.71 g/L Yeast Nitrogen Base-Nitrogen-Niacin (Sunrise Science)), and grown for a further 24 h. Cell pellets were ground with a mortar and pestle in a liquid nitrogen-cooled environment, lysed in 0.2 M NaOH, 0.5% CTAB, and 1/5 cell volume acid-washed beads (212–300 μm;

Sigma-Aldrich) by vortexing. After centrifugation, the supernatant was neutralized in equal parts with 0.5 M TRIS-HCl pH 6.8. Finally, lysates were assessed for total NAD via an enzymatic cycling reaction in which diaphorase catalyzes the conversion of resazurin to the fluorescent resorufin, as described (Graeff & Lee, 2002). Reaction mix was made in water containing 100 mM TRIS-HCl pH 8, 5% ethanol, 0.5 mg/mL bovine serum albumin, 0.5% NP-40, 10 μM riboflavin mononucleotide, 15 U/mL alcohol dehydrogenase, 0.56 U/mL diaphorase, and 32 μM resazurin. Excitation$_{540nm}$/emission$_{590nm}$ measurements were taken every 2 min for 12 min, using a PHERAstar FS Microplate Reader (BMG Labtech), and compared to NAD standards made through serial dilution at known concentrations. Enzymatic activity was assessed in duplicate and normalized to total protein concentrations, assessed by Pierce BCA Protein assay (Thermo Fisher Scientific) according to the manufacturer's instructions. Identical yeast culturing and lysate assessment was performed for *Δbna5* KYNU, p.(His263Arg), p.(Glu206Lys), p.(Lys121del), p.(Ser345Arg), p.(Ala164Profs*26), p.(Arg428Trp), p.(Thr198Ala), p.(Val57Glufs*21), and HAAO yeast. Statistical comparisons of total NAD normalized to total protein concentration were made with GraphPad Prism software using one-way ANOVA with Holm-Sidak multiple comparisons test.

2.7 | Quantitative real-time PCR

All yeast cultures were grown for 24 h in plus-niacin media, then RNA was extracted using TRI Reagent (Sigma-Aldrich) (Collart & Oliviero, 2001). Purity ($A_{260}/A_{280} \geq 1.8$) and concentration were measured using the QIAxpert System (Qiagen). One μg total RNA was then converted to cDNA using the QuantiTect Reverse Transcription Kit according to the manufacturer's instructions. qRT-PCR reactions contained 8 ng cDNA, LightCycler 480 SYBR Green 1 Master (Roche), and forward and reverse primers (0.3 μM). The amplification protocol consisted of 95°C for 3 min, 39 cycles of 95°C for 10 s, and 60°C for 30 s, finished with a standard melting curve protocol. Melting curve analysis and quantification were performed using CFX384 software (BioRad). Each primer was validated to be specific for the gene by confirmation of a single peak on the melting curve. Raw values were exported to Microsoft Excel for analysis of relative quantification using a standard curve. Primers are listed in Table S1. Primers and validation for housekeeping genes *TAF10* and *KRE11* were as previously described (Teste et al., 2009).

3 | RESULTS

Seven probands in unrelated families were identified with potentially pathogenic biallelic variants in *HAAO* or *KYNU* with congenital malformations consistent with Congenital NAD Deficiency Disorder (OMIM: 617660, 617661, 618845). These patients were from unselected groups requiring clinical genetic assessment.

3.1 | Clinical features of patients carrying *HAAO* variants

Three unrelated patients were identified with rare, predicted-deleterious biallelic *HAAO* variants inherited from asymptomatic, non-consanguineous parents (Figure 1). All three probands had diverse congenital heart defects (Table 1), including Tetralogy of Fallot, Shone syndrome, and hypoplastic left heart. The probands of Family (F) 1 (F1.II.8) and Family 3 (F3.II.3) both exhibited limb defects manifesting in abnormal digits of the hands and feet and relatively shortened limbs. These probands also had vertebral anomalies with hemivertebrae and either scoliosis or rib defects. Finally, phenotypes unique to each patient included an absent left kidney and multicystic right kidney, small bladder (F3.II.3), progressive intrauterine growth retardation (F2.II.1), and mild facial dysmorphism (F1.II.8). Due to the phenotypic severity observed in patient F3.II.3, this pregnancy was terminated.

3.2 | Clinical features of patients carrying *KYNU* variants

Four unrelated patients were identified with rare predicted-deleterious biallelic *KYNU* variants inherited from asymptomatic parents (Figure 2). All four probands exhibited limb defects (Table 1), including shortening of the upper and lower extremities, absent digits and nails on the hands and feet, brachymelia, and variable syndactyly. The next most commonly occurring defect in three probands affected the heart in the form of Tetralogy of Fallot with absent pulmonary valve, atrial and ventricular septal defects, aortic hypoplasia, and mitral valve stenosis. These three probands also exhibited mild facial dysmorphism, including wide-spaced eyes, a short and broad neck, microretrognathia, a broad nose with anteverted nares, and abnormally shaped ears. Both F5.II.1 and F6.II.4 were recorded with developmental delay. Phenotypes unique to each patient included an absent left kidney, segmentation errors of the vertebral, thoracic and lumbar spine, fewer ribs with proximal rib fusions, lung hypoplasia, a small stomach, tracheoesophageal fistula (F4.II.2), microcephaly, autism (F5.II.1), growth restriction, cleft palate, cutis marmorata, abnormalities of the iris (F6.II.4), and ventriculomegaly (F7.II.2).

Detailed descriptions and images of individuals with biallelic *HAAO* or *KYNU* variants are presented in Supporting Information: Clinical Histories and Figure S1, respectively.

3.3 | Identification of *HAAO* and *KYNU* variants

Biallelic *HAAO* (NM_012205.3) and *KYNU* (NM_003937.3) variants were identified in all probands through exome or genome sequencing analysis of parent-child trios. Variant rarity and predicted *in silico* pathogenicity metrics are presented in Table 2. All variants scored >20 with respect to CADD-PHRED (Rentzsch et al., 2018), except for

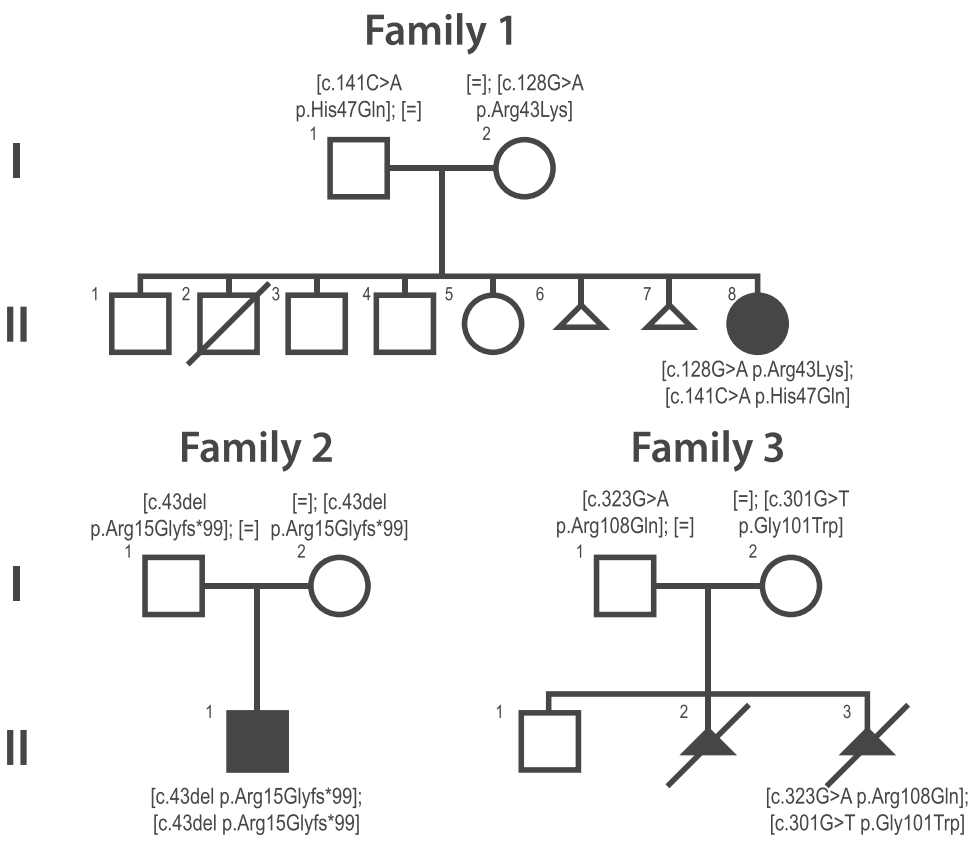

FIGURE 1 Pedigrees of families harboring biallelic *HAAO* variants

KYNU c.361_363del p.(Lys121del), which is close below this threshold (18.25), placing them in the top 1% of deleterious variants. In addition, all missense variants are considered possibly damaging according to M-CAP (Jagadeesh et al., 2016) with a score >0.025 except for *KYNU* c.616G>A p.(Glu206Lys) with a score of 0.0007. The majority of these variants are novel with respect to individuals lacking pediatric disease in the gnomAD database with the rest occurring in fewer than 20 individuals; no variant was present in the homozygous state (Karczewski et al., 2020).

The HAAO variants all occurred within the N-terminal cupin fold protein domain (Figure 3a). Patients 1 (F1.II.8) and 3 (F3.II.3) are each compound heterozygous for two missense variants (c.128G>A p.(Arg43Lys);c.141C>A p.(His47Gln) and c.301G>T p.(Gly101Trp); c.323G>A p.(Arg108Gln), respectively), and patient 2 (F2.II.1) is homozygous for a frameshift (c.43del p.(Arg15Glyfs*99)). All *HAAO* missense variants are predicted pathogenic with respect to PolyPhen-2 HVAR (Adzhubei et al., 2013) with a score ≥0.999, affect highly conserved residues as reflected in GERP rejected substitution scores >4.5 (Davydov et al., 2010), and are not present in the gnomAD database. The only frameshift variant (c.43del p.(Arg15Glyfs*99)), while unable to be compared via the same *in silico* predictors, is similarly rare with a single heterozygous carrier in gnomAD.

In contrast, KYNU variants occurred mostly within the aminotransferase domain without clustering (Figure 3b). Patient 4 (F4.II.2) and 5 (F5.II.1) are homozygous for missense variants (c.788A>G p.(His263Arg) and c.616G>A p.(Glu206Lys), respectively), patient 6 (F6.II.4) is compound heterozygous for a missense (c.1035T>A p.(Ser345Arg)) and an in-frame deletion (c.361_363del p.(Lys121del)), and patient 7 (F7.II.2) is compound heterozygous for a frameshift (c.489del p.(Ala164Profs*26)) and a missense (c.1282C>T p.(Arg428Trp)). An individual with an identical missense change to F7.II.2 *in trans* with a multi-exon *KYNU* deletion (delEx1-8; arr [GRCh37]2q22.2(143,634,577-143,719,262)x1) has been previously identified with phenotypes resembling Congenital NAD Deficiency Disorder (Ehmke et al., 2020). Similar to variants in *HAAO*, all *KYNU* missense variants are predicted pathogenic with respect to PolyPhen-2 HVAR scoring >0.99, except for c.616G>A p.(Glu206Lys) (0.001). These variants also affect conserved residues reflected in GERP rejected substitution scores >2, except for c.1282C>T p.(Arg428Trp) (−0.425), and occur in <0.002% of individuals in gnomAD without any tolerated homozygotes.

In summary, all *HAAO* and *KYNU* variants identified in affected patients are rare with respect to gnomAD (a reference population data set free of pediatric disease) and are predicted damaging by at least three of four *in silico* prediction algorithms.

3.4 | *HAAO* variants result in NAD deficiency

The pathway for the *de novo* synthesis of NAD from L-tryptophan is largely conserved from bacterium to humans. Like vertebrate HAAO, yeast orthologous protein Bna1 (Bna1p) converts

TABLE 1 Phenotypes of patients with biallelic *KYNU* (NM_003937.3) and *HAAO* (NM_012205.3) variants

Family	Patient [variant]	Sex	Vertebral	Cardiac	Renal	Limb	Other
(*HAAO*) F1	II.8 [c.128G>A p.(Arg43Lys)]; [c.141C>A p.(His47Gln)]	Female	L2 hemivertebra; sacral vertebral anomalies; 11 pairs of ribs	Tetralogy of Fallot with complete atrioventricular canal and pulmonary stenosis; persistent LSVC and left pulmonary artery arising from the ductus arteriosus		Clinodactyly of digits 2 and 5 with short middle phalanges on the right hand, clinodactyly of the 5th digit on the left hand, overlapping 1st and 2nd toes	Mild facial dysmorphism (bitemporal narrowing, epicanthic folds and a flat nasal bridge, absent tragi of the ears)
(*HAAO*) F2	II.1 [c.43del p.(Arg15Glyfs*99)]; [c.43del p.(Arg15Glyfs*99)]	Male	-	Shone syndrome with aortic coarctation	-	-	Progressive intrauterine growth retardation
(*HAAO*) F3	II.3 [c.301G>T p.(Gly101Trp)]; [c.323G>A p.(Arg108Gln)]	Male	L5 hemivertebra, scoliosis	Hypoplastic left heart	Absent left kidney, multicystic right kidney	Abnormal hand (right hand: 4–5 syndactyly, abnormal orientation of the hand, flexion contracture of the 3rd digit)	Small bladder
(*KYNU*) F4	II.2 [c.788A>G p.(His263Arg)]; [c.788A>G p.(His263Arg)]	Male	Nine ribs, bilaterally; multiple proximal fusions, lower three pairs of ribs; multiple segmentation errors of the vertebral, thoracic, and lumbar spine; hypoplastic sacrum	Tetralogy of Fallot (absent pulmonary valve), abnormal fusion of right posterior semicircular canal	Absent left kidney	Upper and lower limbs appear short; prominent pterygia at shoulders, elbows, and wrists; clenched hands with overlapping fingers, mild brachymelia	Craniofacial dysmorphism (squared facial profile, short neck with webbing; low anterior hairline, prominent brow; nose broad and flat with anteverted nares; posteriorly angled ears; microretrognathia; ankloglossia), excess wrinkled skin; hypoplastic right lung; small stomach; polyhydramnios (tracheoesophageal fistula)
(*KYNU*) F5	II.1 [c.616G>A; p.(Glu206Lys)]; [c.616G>A; p.(Glu206Lys)]	Female	-	Perimembranous ventricular septal defect, pulmonary vein stenosis	-	Reduction defects (right-hand transverse terminal limb reduction, rudimentary 5th digit; left hand hypoplastic deep-set nails in digits 1/2/3/5; right foot digits 1 + 5 have no nails; digits 2/3/4 absent; left foot digits 3/4/5 are absent (no bones), digits 1 + 2 have no nails, syndactyly)	Microcephaly, global developmental delay, autism, craniofacies (brachycephalic, flat occiput, bitemporal narrowing, normoteloric with normal eyebrows, small nose with a normal philtrum, ears cupped and prominent), bilateral inguinal hernias
(*KYNU*) F6		Female	-	-	-		

(Continues)

TABLE 1 (Continued)

Family	Patient [variant]	Sex	Vertebral	Cardiac	Renal	Limb	Other
	II.4 [c.361_363del p.(Lys121del)]; [c.1035T>A p.(Ser345Arg)]					Cutaneous syndactyly of upper and lower extremities (digits 3–4 (right hand), digits 3–5 (left hand; 2/3 toe syndactyly), short limbs	Growth restriction, developmental delay, cleft palate, cutis marmorata, mild facial dysmorphism (short midface, upturned nose, thin lips, brachycephaly, high anterior hairline, short palpebral fissures, thick nasal alae), ocular crystals, flat iris nodules, uniform hypopigmented patches of the iris bilaterally
(*KYNU*) F7	II.2 [c.489del p.(Ala164Profs*26)]; [c.1282C>T p.(Arg428Trp)]	Female	-	Aortic hypoplasia, atrial septal defect, ventricular septal defect, mitral valve stenosis, dilatation of the pulmonary trunk and ductus arteriosus	-	Shortening of all extremities	Mild facial dysmorphism, hypertelorism, prominent folds at the inner sides of the eyes, ventriculomegaly with unaffected cerebellum

3-hydroxyanthranilic acid to 2-amino-3-carboxymuconate semi-aldehyde (Kucharczyk et al., 1998), which is converted downstream to NAD as the final catabolic product of this pathway. Therefore, we sought to functionally assess human *HAAO* variants via a genetic complementation approach in yeast.

First, yeast homozygous for deletion of *BNA1* (*Δbna1* yeast) were transformed with plasmids generating human wild-type (WT) HAAO, HAAO Arg43Lys, His47Gln, Arg15Glyfs*99, Gly101Trp, or Arg108Gln mutants, or KYNU as a control. Although *BNA1* is not an essential gene in *Saccharomyces cerevisiae*, *BNA1* deletion yeast strains exhibit negligible growth in niacin-free liquid cultures, which can be rescued via complementation with plasmid-expressed *BNA1*. Alternatively, exogenous niacin supplementation may overcome metabolic block induced by *BNA1* deletion, thereby rescuing growth rates (Kucharczyk et al., 1998).

Correspondingly, all yeast cultures grew equivalently well in niacin-supplemented conditions (data not shown), and each mutant was equivalently expressed between strains (Figure S2A) relative to well-established internal reference gene *KRE11* (Teste et al., 2009). To next assess the capacity of human HAAO to compensate for the loss of Bna1p, *Δbna1* yeast generating WT HAAO (*Δbna1* HAAO) were grown in liquid cultures in the absence of niacin for 24 h. We have previously shown that NAD deficiency caused by a metabolic block of the *de novo* NAD biosynthesis pathway in yeast results in compromised cell growth (Szot et al., 2020). Here, *Δbna1* yeast mass relative to WT HAAO was significantly smaller in all mutant cases (38-81% of WT HAAO control; Arg43Lys, His47Gln, Arg15Glyfs*99, Gly101Trp, Arg108Gln, and nonrescue control KYNU; Figure S3A), indicative of compromised growth.

Finally, to determine if NAD deficiency was the cause of altered growth between *Δbna1* WT and HAAO mutants, we compared total NAD (NAD^+ and NADH) in cell lysates (Szot et al., 2020). *Δbna1* WT and HAAO mutants were initially grown in plus-niacin conditions, subsequently transferred to and grown in minus-niacin media for a further 24 h, lysed, and their NAD concentration determined. Total cellular NAD for *Δbna1* KYNU was considered baseline because this protein cannot rescue the functionality of yeast Bna1p (Figure 4a). NAD levels in each yeast strain generating a HAAO mutant were significantly decreased 2–17-fold compared to wild-type *Δbna1* HAAO (Arg43Lys, His47Gln, Arg15Glyfs*99, Gly101Trp, Arg108Gln; Figure 4a), suggesting that their compromised growth in un-supplemented conditions was a result of perturbed HAAO enzymatic activity.

In summary, all human *HAAO* variants identified in patients resulted in reduced growth and total NAD levels in yeast.

3.5 | *KYNU* variants result in NAD deficiency

Yeast orthologous protein to vertebrate KYNU (Bna5p) is also functionally conserved within the *de novo* NAD synthesis pathway from L-tryptophan, acting directly before Bna1p and catalyzing the generation of 3-hydroxyanthranilic acid from L-3-hydroxykynurenine

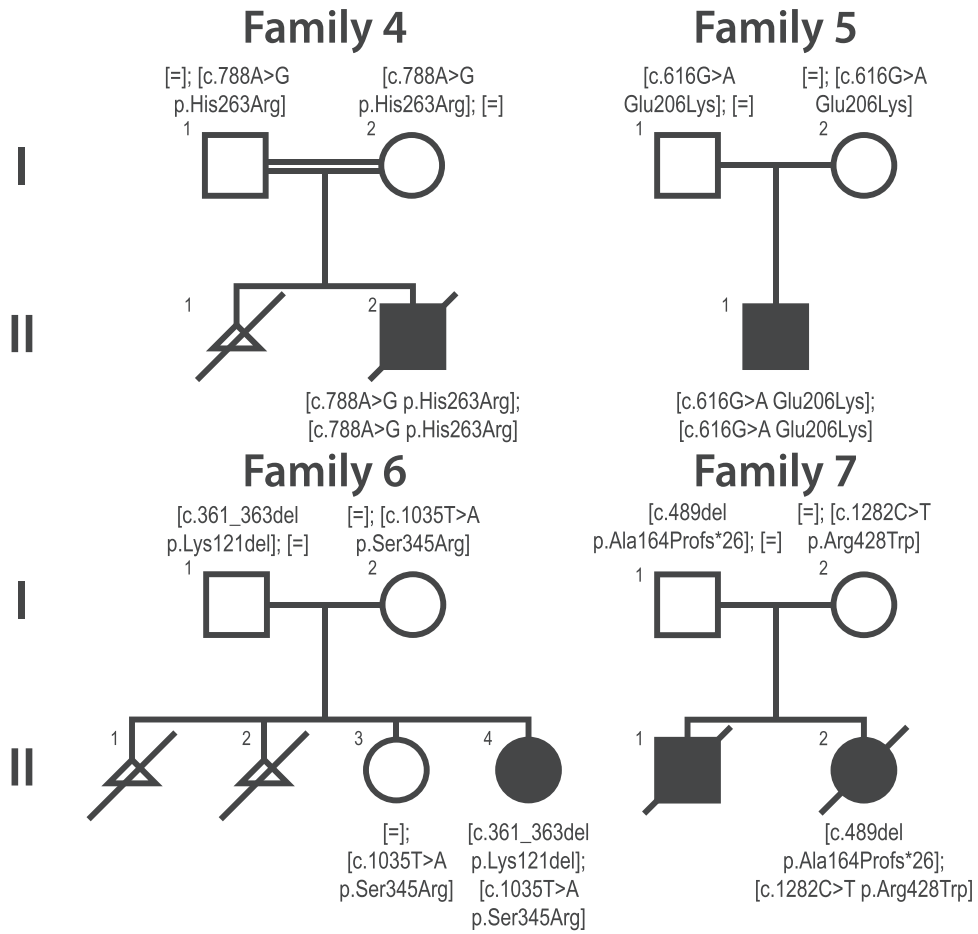

FIGURE 2 Pedigrees of families harboring biallelic *KYNU* variants

TABLE 2 *HAAO* (NM_012205.3) and *KYNU* (NM_003937.3) variants identified in affected patients and their predicted pathogenicity

Patient	cDNA change	Predicted protein change	PolyPhen-2 HVAR	CADD-PHRED	M-CAP	GERP (RS)	Heterozygous count in gnomAD (frequency)
HAAO F1	128G>A	Arg43Lys	1	25.3	0.052	4.56	0 (0)
HAAO F1	141C>A	His47Gln	1	24.9	0.132	4.57	0 (0)
HAAO F2	43del	Arg15Glyfs*99	n/a	26.4	n/a	n/a	1 (0.00000443)
HAAO F3	301G>T	Gly101Trp	1	28.3	0.215	4.69	0 (0)
HAAO F3	323G>A	Arg108Gln	0.999	27.5	0.121	4.69	0 (0)
KYNU F4	788A>G	His263Arg	0.992	25.7	0.042	6.07	0 (0)
KYNU F5	616G>A	Glu206Lys	0.001	23.2	0.0007	5.35	5 (0.0000199)
KYNU F6	361_363del	Lys121del	n/a	18.25	n/a	2.42	5 (0.0000177)
KYNU F6	1035T>A	Ser345Arg	0.99	25.5	0.081	3.49	0 (0)
KYNU F7	489del	Ala164Pfs*26	n/a	32	n/a	n/a	19 (0.0000674)
KYNU F7	1282C>T	Arg428Trp	1	23.4	0.054	−0.425	18 (0.0000717)

Note: PolyPhen-2 HVAR (Adzhubei et al., 2010): Score ≥ 0.909: probably damaging; 0.908 ≤ score ≤ 0.447: possibly damaging; score ≤ 0.446: benign. CADD-PHRED (Rentzsch et al., 2018): scaled CADD score ≥ 15: damaging; M-CAP (Jagadeesh et al., 2016): possibly damaging >0.025; GERP++ (Davydov et al., 2010), >2: evolutionarily constrained; gnomAD (Karczewski et al., 2020).

Abbreviation: n/a: not applicable.

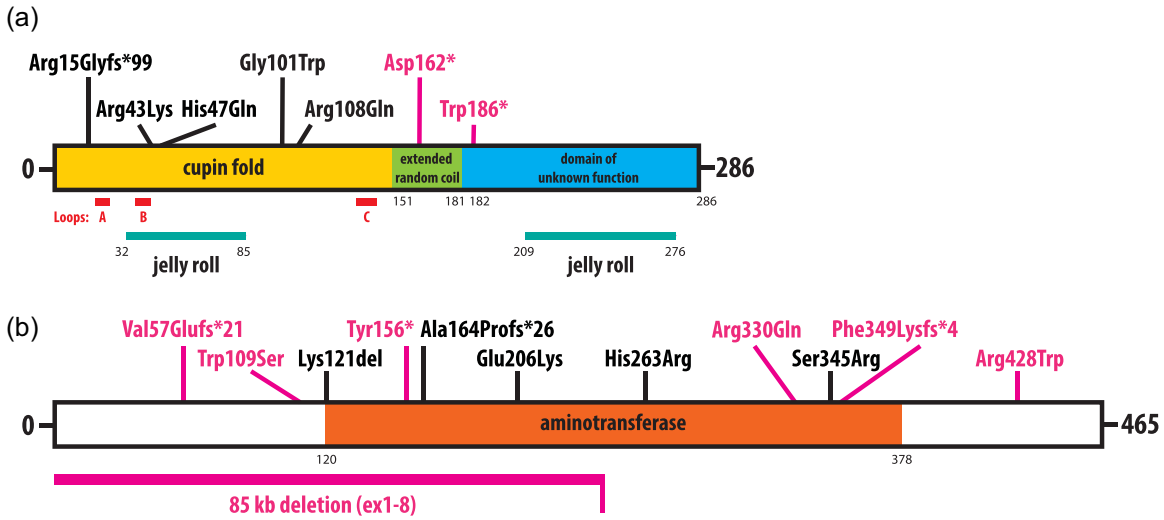

FIGURE 3 Protein domain diagrams of human HAAO and KYNU highlighting the positions of variants identified in individuals. (a) HAAO missense and frameshift variants in black are reported here. Conserved loops regions A [AA 17–25], B [AA 36–43], and C [AA 134–143] are highlighted in red. Variants in pink have been previously reported (Shi et al., 2017). (b) KYNU missense and frameshift variants in black are reported here. Variants in pink have been previously reported (Ehmke et al., 2020; Shi et al., 2017). Arg428Trp has been identified here and previously reported (Ehmke et al., 2020)

(Panozzo et al., 2002). In this manner, Bna5p and Bna1p exhibit sequential enzymatic activity synthesizing NAD as the catabolic endpoint. Therefore, we also sought to assess the effect of *KYNU* variants in this model system.

Yeast homozygous for deletion of *BNA5* (*Δbna5* yeast) were transformed with plasmids generating human wild-type (WT) KYNU, KYNU His263Arg, Glu206Lys, Lys121del, Ser345Arg, Ala164-Profs*26, Arg428Trp, Thr198Ala, Val57Glufs*21, or HAAO as a control. Two siblings with homozygous KYNU Thr198Ala variants had been identified with hydroxykynureninuria but without congenital malformations (Christensen et al., 2007). In addition, as enzymatic assessment revealed mutant KYNU activity to be 64%

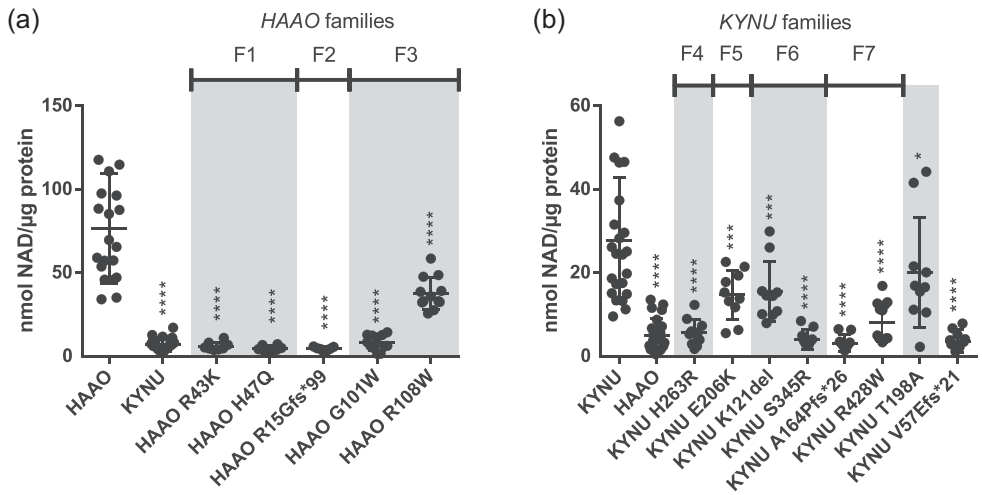

FIGURE 4 Genetic complementation of yeast orthologs with human HAAO or KYNU, their mutant counterparts, and respective levels of total synthesized NAD^+/H. (a) *Δbna1* WT HAAO and mutants Arg15Glyfs*99, Arg43Lys, His47Gln, Gly101Trp, Arg108Gln, or KYNU control yeast, seeded at $OD_{600\,nm}$ 0.15, were grown in the absence of niacin for 24 h. Total NAD^+/H concentrations in yeast lysates were then normalized to protein lysate. ****$p < .0001$. Horizontal bars indicate mean and standard deviation. Statistical comparisons indicate one-way ANOVA comparing mean values of WT HAAO to mutant cases. (b) *Δbna5* WT KYNU, and mutants His263Arg, Glu206Lys, Ser345Arg, Lys121del, Ala164Profs*26, Arg428Trp, Thr198Ala, Val57Glufs*21, or HAAO control yeast, seeded at $OD_{600\,nm}$ 0.15, were grown in the absence of niacin for 24 h. Total NAD^+/H concentrations in yeast lysates were then normalized to protein lysate. *$p < .05$, ***$p < .001$, ****$p < .0001$. Horizontal bars indicate mean and standard deviation. Statistical comparisons indicate one-way ANOVA comparing mean values of WT KYNU to mutant cases. F, family

that of the wild-type protein (Shi et al., 2017), this mutant was therefore included as an internal disease-negative control. Val57-Glufs*21 was also included as a LOF control previously identified in a family with Congenital NAD Deficiency Disorder (Shi et al., 2017).

Similar to *Δbna1* yeast, all *Δbna5* yeast cultures grew equivalently well in plus-niacin conditions (data not shown), and each mutant was equivalently expressed between strains relative to well-established reference gene *TAF10* (Teste et al., 2009) besides *KYNU* Val57Glufs*21 and *HAAO*, which exhibited higher expression (Figure S2B). To next assess the capacity of human *KYNU* to compensate for the loss of Bna5p, *Δbna5* yeast generating WT KYNU (*Δbna5* KYNU) were grown in liquid cultures in the absence of niacin for 24 h. Total *Δbna5* yeast mass relative to WT KYNU was significantly decreased in six of nine mutant strains (21-70% of WT KYNU control; His263Arg, Ala164Profs*26, Val57Glufs*21, Ser345Arg, Arg428Trp, and nonrescue control HAAO; Figure S3B). These observations were indicative of compromised growth.

Total NAD was then determined in cell lysates of *Δbna5* KYNU and mutant yeast grown in the absence of niacin. Compared to wild-type *Δbna5* KYNU, all tested KYNU mutants had significantly reduced total NAD (His263Arg, Glu206Lys, Lys121del, Ser345Arg, Ala164Profs*26, Arg428Trp, Val57Glufs*21, Thr198Ala; Figure 4b). Total NAD for Thr198Ala mutation was reduced to 74% of WT, comparable to enzymatic levels in previously reported assessment (Shi et al., 2017). Total cellular NAD for *Δbna5* HAAO is considered baseline because this protein cannot rescue the functionality of yeast Bna5p (Figure 4b). This finding revealed that KYNU variants identified in all four families caused significant NAD reduction in yeast lysates, 57% or below that of WT KYNU, indicative of impaired protein function.

In summary, all human *KYNU* variants identified in patients resulted in significantly reduced total NAD levels in yeast, and most mutants reduced yeast growth.

4 | DISCUSSION

Here, we report that seven unrelated patients with phenotypes consistent with Congenital NAD Deficiency Disorder carry biallelic variants in *HAAO* or *KYNU* with lost or reduced function. To date, two variants in *HAAO* and three variants in *KYNU* (all protein-truncating), have been directly functionally assessed by determining enzymatic activity in vitro or phenotypically by analyzing embryos of genetically modified mouse models (Shi et al., 2017). Additionally, the functional analysis of variants has also been indirectly assessed by quantifying metabolites upstream and downstream of KYNU and HAAO in the *de novo* NAD biosynthesis pathway, including NAD (Shi et al., 2017). These approaches vary in complexity and practicality. Here, we showed that each of the five *HAAO* or six *KYNU* variants (two protein-truncating) predicted to alter protein function, significantly reduced downstream NAD levels in yeast. We predict that impaired enzyme function reduced NAD synthesis in these patients below a threshold resulting in disrupted embryogenesis.

All three patients with biallelic *HAAO* variants exhibited defects consistent with previously published patients (Table S2). The most commonly occurring malformations affect the heart (5/5), while slightly less common were those of the vertebrae (4/5), limbs (3/5), and kidneys (3/5). This observation is generally in agreement with studies of homozygous LOF *HAAO* mouse models in which embryos of this genotype consistently developed multiple malformations of the vertebrae, heart, kidney, digits, palate, and limbs (Cuny et al., 2020; Shi et al., 2017). Biallelic LOF *HAAO* patients have previously been recorded with elevated levels of HAAO substrate 3-hydroxyanthranilic acid at least 64 times the mean of healthy controls, indicative of metabolic block caused by HAAO inactivation, and consequently at most one-third the NAD levels of healthy counterparts (Shi et al., 2017). While metabolic data are unavailable for F1.II.8 and F3.II.3, F2.II.1 was documented with similarly elevated levels of 3-hydroxyanthranilic acid 45 times the mean of healthy controls, indicative of comparably impaired HAAO activity within the *de novo* NAD biosynthesis pathway.

Mechanistically, HAAO has been shown to adopt two alternate conformations depending on the arrangement of three conserved hydrophobic loop regions (Figure 3a) enclosing the catalytic ferrous iron center: a substrate-free "open" conformation, or a substrate-bound "closed" conformation. In the open conformation, the active site is exposed from opposing directions similar to a tunnel for passive substrate diffusion. Upon substrate binding, the three loops converge to surround the catalytic core, creating a significantly more compact and hydrophobic environment, heightening the attraction for molecular oxygen (Yang et al., 2018). Coordinated oxygen incorporation is key to overall enzyme activity as oxygen exposure in the open conformation oxidizes the metal ion (to Fe^{3+}) and inactivates the enzyme (Colabroy et al., 2005), and variants impairing loop movement when establishing the hydrophobicity of the closed conformation comparably exhibit basal catalytic efficiency (Yang et al., 2018).

All *HAAO* missense variants reported here occur within the N-terminal cupin fold domain, which spans loops A, B, and C (Figure 3a). Both residues affected in F1.II.8 (Arg43 and His47) have been previously studied in HAAO orthologs with purported necessary functions within the active site. Arg43 is hydrogen-bonded to Asp45 and comprises a positively charged region at the edge of the substrate entering hatch (Loop B), directly stabilizing the transition state of Fe^{2+} to Fe^{3+}. Computer-simulated mutation to alanine halves enzymatic activity (Brkic et al., 2015) and equivalent mutation in vitro exhibits substrate inhibition (Zhang et al., 2005). It is therefore likely that mutation to lysine (Arg43Lys, F1.II.8) similarly loses stability and eases Fe^{2+} oxidation, thereby inactivating the enzyme in the open conformation. His47 and His91 each contribute a nitrogen ligand, alongside a bidentate interaction from Glu53, to coordinate central Fe^{2+} at the active site (Pidugu et al., 2017; Zhang et al., 2005). Perturbing this interaction via mutation to glutamine (His47Gln, F1.II.8) will likely lose this interaction and consequently lose enzymatic activity. Residues affected in F3.II.3 (Gly101 and Arg108) are less well functionally established yet both occur within the jelly roll

of the cupin fold. According to the crystal structure of human HAAO (Pidugu et al., 2017), Gly101 is situated within a β-sheet directly adjacent to Loop B, enclosing the catalytic site. Mutation to the large aromatic tryptophan (Gly101Trp, F3.II.3) may impact enzyme activity by disrupting the movement of this loop. Arg108 forms a part of a highly conserved hydrogen-bonding network alongside His47, Glu105, and Asp114 with ends linking the catalytic iron (Zhang et al., 2005). Similar to simulated mutation of His47 or Glu105, glutamine mutation at Arg108 (Arg108Gln, F3.II.3) might alter substrate-binding kinetics such that oxygen binding at the catalytic site is less favored, thereby reducing overall enzyme activity (Brkic et al., 2015). Correspondingly, all HAAO variants result in a significant reduction of total synthesized NAD downstream, proportional to their impaired growth, in yeast (Table S2).

All four patients with biallelic *KYNU* variants exhibited defects consistent with both previously published patients (Table S2), with malformations most commonly affecting the limbs (6/6) and heart (5/6), while half of the cases exhibit vertebral (3/6) and kidney (3/6) defects. These observations are in agreement with *KYNU* knockout mouse embryos, which develop multiple malformations of the limbs, heart, vertebrae, kidney, palate, and digits (Shi et al., 2017). A patient with biallelic LOF *KYNU* variants has previously been recorded with elevated levels of KYNU substrate 3-hydroxykynurenine 161 times greater than the mean of healthy controls, indicative of metabolic block caused by KYNU inactivation, and one-seventh the NAD levels of healthy counterparts (Shi et al., 2017). While metabolic data are not available for any *KYNU* patients reported here, a patient genotypically equivalent to that of F7.II.2 (delEx1-8; c.1282C>T p.(Arg428Trp) (Ehmke et al., 2020)) was documented with 3-hydroxykynurenine levels 55 times greater than that of healthy controls, similarly indicative of kynureninase dysfunction and probable NAD deficiency.

KYNU is a member of the aminotransferase superfamily of PLP-dependent enzymes. These enzymes have a fold with a large domain that binds PLP and a mobile small domain that can close the active site during catalysis (Figure S4). At a protein level, His263 is found on a β-turn at the surface of KYNU and its mutation is unlikely to affect the activity by active site disruption. However, His263 is conserved in the structures of KYNU from humans (Lima et al., 2007) and bacteria (*Pseudomonas fluorescens*) (Momany et al., 2004), suggesting an important function. Mutation of this residue to arginine (His263Arg, F4.II.2) may affect the dynamics of conformational changes required during catalysis. The hydroxyl group of Ser345 donates a hydrogen bond to the carbonyl oxygen of Lys278. Loss of this hydrogen bond in the Ser345Arg mutant (F6.II.4) is likely to affect the environment of Lys276, which is covalently attached to the PLP cofactor. Ser345 is not conserved and is replaced by Gly in the *P. fluorescens* structure. Arg428 is in the small domain of KYNU, where it forms a salt bridge with Glu197 on a loop in the large domain. Since the small domain is mobile and moves toward the large domain to close the active site when substrate binds (Lima et al., 2007), the Arg428Trp mutation (F7.II.2) likely affects the mobility of the small domain. Consistent with this possibility, Arg428 is conserved in the *P. fluorescens* KYNU structure. Thr198 is also located on the loop next to Glu197, which interacts with Arg428. Therefore, the Thr198Ala mutation (Christensen et al., 2007) may have a similar effect to the Arg428Trp mutation. Glu206 and Lys121 are located on the surface of the protein remote from the active site, so it is unclear how their mutation (Glu206Lys, F5.II.1; Lys121del, F6.II.4) significantly affects activity. Similar to variants in HAAO, all KYNU variants exhibit significantly reduced total NAD, with all predicted disease-causal variants in patients synthesizing NAD below that of non-disease-causal variant Thr198Ala (Table S2).

To date, all *HAAO* or *KYNU* variants identified as causal of Congenital NAD Deficiency Disorder are complete LOF due to changes in mRNA reading frame and protein truncation (Shi et al., 2017). Here, we identify multiple rare damaging missense changes in *HAAO* or *KYNU* that result in moderate to complete LOF and NAD deficiency. Generally, the more severely compromised NAD synthesis in yeast caused by these variants, the greater number of malformations observed in affected patients (Table S2). Within a specific organ structure, however, there is significant variation in the severity of defect that does not directly correlate with the degree of NAD deficiency. For example, cardiac malformations range from septal defects to hypoplastic left heart while kidneys are unaffected or entirely undeveloped. In *KYNU* patients with the least damaging variants causing mild NAD deficiency (F5.II.1, KYNU Glu206Lys; F6.II.4, KYNU Ser345Arg; Lys121del), renal and vertebral defects are not observed, suggesting potentially a dosage-sensitive susceptibility for various organs to the levels of NAD during embryogenesis.

Both F5.II.1 and F6.II.4 harbor additional gene variants, which may partially explain their distinct phenotypes, despite their suspected relatively mild NAD deficiency caused by *KYNU* mutation. F6.II.4 and sibling F6.II.3 both exhibited cleft palate. Although the cleft palate is a feature of Congenital NAD Deficiency Disorder, it may be explained by an inherited variant in NM_001329630.1(*PLEKHA7*):c.571G>A p.(Asp191Asn), a gene recently linked with non-syndromic cleft palate (Cox et al., 2018). F6.II.4 also inherited a 22q11.21 duplication from her father (F6.I.1) who was recorded with learning difficulties. This duplication has been associated with developmental delay and cognitive deficits, which have been observed in this patient (Wentzel et al., 2008). F5.II.1 carries a homozygous LOF variant in NM_153332.4(*ERI1*):c.514C>T p.(Gln172*), a gene which has previously been identified in a homozygous microdeletion encompassing an additional gene *MFHAS1* in a patient with similar limb and cardiac abnormalities to F5.II.1 (Choucair et al., 2017). Whereas the functional link between *ERI1* mutation and these defects remains to be assessed, the impact of these additional variants may confound the contribution of mild NAD deficiency observed in these two patients.

Variants inactivating either *HAAO* or *KYNU* may be expected to cause equivalent anomalies in humans because of a common deficiency in NAD synthesis. This is almost entirely observed in isogenic mice homozygous-null for either *HAAO* or *KYNU* on restricted diets, exhibiting consistent malformations of the kidneys, tail, limbs, and

vertebrae, with minor variation in defects of the heart, digits, and palate (Shi et al., 2017). In humans with biallelic variants in *HAAO* or *KYNU*, significant phenotypic variation exists among individuals of the same genotype. This is seen in the comparison of F7.II.2 (KYNU Ala164Profs*26;Arg428Trp), which we show to be severely NAD deficient (Figure 4b), to a prior pregnancy in the same family terminated due to considerable congenital malformation (F7.II.1). Due to their phenotypic overlap concerning craniofacial anomalies and defects of the heart and limbs, it is likely that F7.II.1 shares an equivalent *KYNU* genotype. However, this individual additionally exhibited vertebral, kidney, and palatal defects (Supporting Information), suggesting the influence of additional genetic or environmental factors or both modulating the severity of NAD deficiency, as shown by the effect of diet in mice (Cuny et al., 2020). Moreover, a patient with a functionally equivalent *KYNU* genotype (delEx1-8; Arg428Trp) exhibits defects similar to F7.II.1 with the exception of kidney malformation. While this patient, and two others with presumed homozygous LOF *KYNU* variants, were reported with a form of hand hyperphalangism pathognomonic for Catel-Manzke syndrome (Ehmke et al., 2020), this has not been observed in any NAD-deficient patient identified here nor previously (Shi et al., 2017). In mice, dietary niacin, which enters the *de novo* NAD biosynthesis pathway downstream of either KYNU or HAAO, can entirely overcome metabolic block caused by inactivation of these genes and supplement *de novo* NAD production in sufficient quantity to rescue all NAD-dependent congenital malformation and miscarriage (Shi et al., 2017). It is reasonable to suggest that differences in availability of vitamin B3 (nicotinic acid, niacin, nicotinamide, nicotinamide riboside) may greatly influence NAD levels during gestation and thus phenotypic severity. This situation may explain the comparably minor defects observed in F2.II.1 (HAAO Arg15Glyfs*99) compared to F3.II.3 (HAAO Gly101Trp;Arg108Gln), despite more severely impacted NAD synthesis in vitro (Figure 4a).

Half of the families identified to date with Congenital NAD Deficiency Disorder exhibit miscarriage (Shi et al., 2017; Szot et al., 2020). This is consistent with families identified here, with prior pregnancies of four of seven probands recorded as miscarriages (Figures 1 and 2). For future pregnancies in these families, NAD precursor supplementation may prove useful. Patient F2.II.1 was placed on an NAD precursor supplementation program one-month after birth, receiving 11 mg/kg/day niacin. Although there are no patients with Congenital NAD Deficiency Disorder currently recorded on niacin supplementation, given the established benefit of supplementation in adults (Rajman et al., 2018), and the potential to benefit the speech and developmental delays associated with *HAAO* LOF patients (Shi et al., 2017), it will be interesting to follow the progression of this patient over time. Therapeutic administration of the NAD precursors nicotinamide riboside (Trammell et al., 2016) and nicotinamide mononucleotide (Kim et al., 2020) have been shown to significantly bolster NAD synthesis via the *de novo* pathway via direct or indirect means, respectively, while nicotinamide riboside supplementation in humans has been documented with minimal adverse physiological outcomes (Trammell et al., 2016). The choice between NAD precursors for future therapeutic recommendation is still unclear. However, further studies regarding synergism with the gut microbiome (Shats et al., 2020) and mechanisms of flux through various tissue types (Liu et al., 2018) will need to be considered.

It is still unclear which processes are disrupted by NAD deficiency during embryogenesis. In mice, NAD has been shown to be necessary for the preservation of oocyte quality and improved fertility outcomes, with precursor-based supplementation shown to overcome age-dependent decline (Bertoldo et al., 2020). Depending on the level of NAD deficiency, adverse pregnancy outcomes have been recorded as early as embryonic day 4.5 (equivalent to day 5 in humans) (Shi et al., 2017) with developmental delay observed by day 9.5 (day 22 in humans) (Cuny et al., 2020). Future studies are required to resolve which individual or collective NAD-dependent processes (ATP production, biosynthesis, DNA repair, stress response, metabolism) contribute to embryonic disruption.

In summary, we have identified seven new cases of Congenital NAD Deficiency Disorder in humans stemming from rare biallelic variants in *HAAO* or *KYNU*, exhibiting multiple malformations consistent with insufficient NAD during embryogenesis. We showed by yeast genetic complementation assays that individual mutations in either gene disrupt NAD synthesis through the *de novo* pathway and reduces NAD levels. The extent and duration of NAD deficiency during human gestation will depend on the availability of vitamin B3 precursors of NAD and the amount of stored NAD in the maternal liver. Our study expands the phenotypic spectrum of defects caused by embryonic NAD deficiency and establishes that missense mutation within HAAO or KYNU can cause malformation due to reduced enzyme activity. Although all patients present with multiple malformations, it has been shown that NAD deficiency, caused by exacerbation of heterozygous NAD biosynthesis gene deletion by environmental factors, can cause isolated congenital defects (Cuny et al., 2020). It is therefore possible that combinations of more common and less damaging gene mutations, sensitive to environmental insult, manifest a more subtle or isolated NAD-dependent phenotype than patients identified to date. Vitamin B3 supplementation might reduce the incidence or severity of NAD deficiency and adverse pregnancy outcomes. Finally, we recommend that unresolved cases of multiple malformations, such as VACTERL association (Stevenson & Hunter, 2013), affecting the limbs, heart, kidneys, or vertebrae, as in cases of biallelic *HAAO* or *KYNU* variation (Table S2), be assessed for biallelic variants in genes of the *de novo* NAD biosynthesis pathway and/or NAD deficiency.

ACKNOWLEDGEMENTS

We thank Dr. Gregory Costain for the assistance in data collection and Dr. Paul Mark for his clinical insights. Anna M. Cueto-González and Eduardo F. Tizzano are affiliated with the European Reference Network on Rare Congenital Malformations and Rare Intellectual Disability, and the European Reference Network for Craniofacial Anomalies and ENT Disorders. The CAUSES Study was made

possible by a $3 million donation from Mining for Miracles through the BC Children's Hospital Foundation and was supported by Genome British Columbia, the Provincial Health Services Authority, BC Children's and Women's Hospitals, The Provincial Medical Genetics Program, BC Children's Hospital Pathology and Laboratory Medicine, and the University of British Columbia. Investigators in the CAUSES Study (Clinical Assessment of the Utility of Sequencing as a Service) include Shelin Adam, Nick Dragojlovic, Christèle du Souich, Alison M. Elliott, Anna Lehman, Larry Lynd, Jill Mwenifumbo, Tanya N. Nelson, Clara van Karnebeek, and Jan M. Friedman (PI). The bioinformatic pipeline used in part of the CAUSES Study was developed in the laboratory of Wyeth Wasserman. We are grateful to the families for participating in this study. This study was supported by the National Health and Medical Research Council Project Grant 1162878 (Sally L. Dunwoodie) and Fellowship 1042002 (Sally L. Dunwoodie), Office of Health and Medical Research of the New South Wales Government (Sally L. Dunwoodie), The Key Foundation (Sally L. Dunwoodie), University of Toronto McLaughlin Centre (D. James Stavropoulos). Research reported in this publication was supported by the National Human Genome Research Institute of the National Institutes of Health under Award Number U01HG009599. The content is solely the responsibility of the authors and does not necessarily represent the official views of the National Institutes of Health.

CONFLICT OF INTERESTS

The authors declare that there are no conflict of interests.

WEB RESOURCES

OMIM: https://www.omim.org/
ClinVar: https://www.ncbi.nlm.nih.gov/clinvar/
CADD: https://cadd.gs.washington.edu/
M-CAP: http://bejerano.stanford.edu/mcap/
gnomAD: https://gnomad.broadinstitute.org/

DATA AVAILABILITY STATEMENT

The HAAO and KYNU variants reported in this manuscript are accessible in ClinVar (https://www.ncbi.nlm.nih.gov/clinvar/) with the submission number SUB8498741. Other research data are not available due to privacy or ethical restrictions.

ORCID

Justin O. Szot http://orcid.org/0000-0001-6513-2352
Anne Slavotinek http://orcid.org/0000-0001-7053-2449
Marjan Nezarati http://orcid.org/0000-0002-3570-2155
Anna M. Cueto-González http://orcid.org/0000-0002-7654-785X
Millan S. Patel http://orcid.org/0000-0001-7061-6837
Walter P. Devine http://orcid.org/0000-0003-4634-8830
Shannon Rego http://orcid.org/0000-0003-1910-7441
Susan Blaser http://orcid.org/0000-0001-8891-5106
Tim V. Mieghem http://orcid.org/0000-0002-3034-6905
Silvia A. Martínez http://orcid.org/0000-0001-8169-1322
Eduardo F. Tizzano http://orcid.org/0000-0002-7116-6310
Lucie Dupuis http://orcid.org/0000-0002-6068-8199
Dimitri James Stavropoulos http://orcid.org/0000-0001-5498-2108
Vanda McNiven http://orcid.org/0000-0001-6185-6177
Roberto Mendoza-Londono http://orcid.org/0000-0003-3542-8106
Alison M. Elliott http://orcid.org/0000-0002-9896-1314
Robert S. Phillips http://orcid.org/0000-0001-8710-562X
Gavin Chapman http://orcid.org/0000-0002-3513-723X
Sally L. Dunwoodie http://orcid.org/0000-0002-2069-7349

REFERENCES

Adzhubei, I., Jordan, D. M., & Sunyaev, S. R. (2013). Predicting functional effect of human missense mutations using PolyPhen-2. *Current Protocols in Human Genetics*, *76*(1), 7.20.1–7.20.41. https://doi.org/10.1002/0471142905.hg0720s76

Adzhubei, I. A., Schmidt, S., Peshkin, L., Ramensky, V. E., Gerasimova, A., Bork, P., Kondrashov, A. S., & Sunyaev, S. R. (2010). A method and server for predicting damaging missense mutations. *Nature Methods*, *7*(4), 248–249. https://doi.org/10.1038/nmeth0410-248

Amberg, D. C., Burke, D. J., & Strathern, J. N. (2006). Yeast colony PCR. *Cold Spring Harbor Protocols*, *2006*(1), prot4170. https://doi.org/10.1101/pdb.prot4170

Ansari, H. R., & Raghava, G. P. (2010). Identification of NAD interacting residues in proteins. *BMC Bioinformatics*, *11*(1), 160. https://doi.org/10.1186/1471-2105-11-160

Bertoldo, M. J., Listijono, D. R., Ho, W. J., Riepsamen, A. H., Goss, D. M., Richani, D., Jin, X. L., Mahbub, S., Campbell, J. M., Habibalahi, A., Loh, W. N., Youngson, N. A., Maniam, J., Wong, A., Selesniemi, K., Bustamante, S., Li, C., Zhao, Y., Marinova, M. B., … Wu, L. E. (2020). NAD(+) repletion rescues female fertility during reproductive aging. *Cell Reports*, *30*(6), 1670–1681. https://doi.org/10.1016/j.celrep.2020.01.058

Brkic, H., Kovacevic, B., & Tomic, S. (2015). Human 3-hydroxyanthranilate 3,4-dioxygenase (3HAO) dynamics and reaction, a multilevel computational study. *Molecular BioSystems*, *11*(3), 898–907. https://doi.org/10.1039/c4mb00668b

Cambronne, X. A., & Kraus, W. L. (2020). Location, location, location: Compartmentalization of NAD+ synthesis and functions in mammalian cells. *Trends in Biochemical Sciences*, *45*, 858–873. https://doi.org/10.1016/j.tibs.2020.05.010

Choucair, N., Rajab, M., Megarbane, A., & Chouery, E. (2017). Homozygous microdeletion of the ERI1 and MFHAS1 genes in a patient with intellectual disability, limb abnormalities, and cardiac malformation. *American Journal of Medical Genetics, Part A*, *173*(7), 1955–1960. https://doi.org/10.1002/ajmg.a.38271

Christensen, M., Duno, M., Lund, A. M., Skovby, F., & Christensen, E. (2007). Xanthurenic aciduria due to a mutation in KYNU encoding kynureninase. *Journal of Inherited Metabolic Disease*, *30*(2), 248–255. https://doi.org/10.1007/s10545-007-0396-2

Colabroy, K. L., Zhai, H., Li, T., Ge, Y., Zhang, Y., Liu, A., Ealick, S. E., McLafferty, F. W., & Begley, T. P. (2005). The mechanism of inactivation of 3-hydroxyanthranilate-3,4-dioxygenase by 4-chloro-3-hydroxyanthranilate. *Biochemistry*, *44*(21), 7623–7631. https://doi.org/10.1021/bi0473455

Collart, M. A., & Oliviero, S. (2001). Preparation of yeast RNA. *Current Protocols in Molecular Biology*, *13*(1), 13.12.1–13.12.5. https://doi.org/10.1002/0471142727.mb1312s23

Cox, L. L., Cox, T. C., Moreno Uribe, L. M., Zhu, Y., Richter, C. T., Nidey, N., Standley, J. M., Deng, M., Blue, E., Chong, J. X., Yang, Y., Carstens, R. P., Anand, D., Lachke, S. A., Smith, J. D., Dorschner, M. O., Bedell, B., Kirk, E., Hing, A. V., … Roscioli, T. (2018). Mutations in the epithelial cadherin-p120-catenin complex cause mendelian non-syndromic cleft lip with or without cleft palate.

American Journal of Human Genetics, *102*(6), 1143–1157. https://doi.org/10.1016/j.ajhg.2018.04.009

Cuny, H., Rapadas, M., Gereis, J., Martin, E., Kirk, R. B., Shi, H., & Dunwoodie, S. L. (2020). NAD deficiency due to environmental factors or gene-environment interactions causes congenital malformations and miscarriage in mice. *Proceedings of the National Academy of Sciences of the United States of America*, *117*(7), 3738–3747. https://doi.org/10.1073/pnas.1916588117

Davydov, E. V., Goode, D. L., Sirota, M., Cooper, G. M., Sidow, A., & Batzoglou, S. (2010). Identifying a high fraction of the human genome to be under selective constraint using GERP++. *PLOS Computational Biology*, *6*(12), e1001025. https://doi.org/10.1371/journal.pcbi.1001025

Ehmke, N., Cusmano-Ozog, K., Koenig, R., Holtgrewe, M., Nur, B., Mihci, E., Babcock, H., Gonzaga-Jauregui, C., Overton, J. D., Xiao, J., Martinez, A. F., Muenke, M., Balzer, A., Jochim, J., El Choubassi, N., Fischer-Zirnsak, B., Huber, C., Kornak, U., Elsea, S. H., … Ferreira, C. R. (2020). Biallelic variants in KYNU cause a multisystemic syndrome with hand hyperphalangism. *Bone*, *133*, 115219. https://doi.org/10.1016/j.bone.2019.115219

Graeff, R., & Lee, H. C. (2002). A novel cycling assay for cellular cADP-ribose with nanomolar sensitivity. *Biochemical Journal*, *361*(Pt 2), 379–384. https://doi.org/10.1042/bj3610379

Jagadeesh, K. A., Wenger, A. M., Berger, M. J., Guturu, H., Stenson, P. D., Cooper, D. N., Bernstein, J. A., & Bejerano, G. (2016). M-CAP eliminates a majority of variants of uncertain significance in clinical exomes at high sensitivity. *Nature Genetics*, *48*(12), 1581–1586. https://doi.org/10.1038/ng.3703

Karczewski, K. J., Francioli, L. C., Tiao, G., Cummings, B. B., Alföldi, J., Wang, Q., Collins, R. L., Laricchia, K. M., Ganna, A., Birnbaum, D. P., Gauthier, L. D., Brand, H., Solomonson, M., Watts, N. A., Rhodes, D., Singer-Berk, M., England, E. M., Seaby, E. G., Kosmicki, J. A., … MacArthur, D. G. (2020). The mutational constraint spectrum quantified from variation in 141,456 humans. *Nature*, *581*(7809), 434–443. https://doi.org/10.1038/s41586-020-2308-7

Katsyuba, E., Romani, M., Hofer, D., & Auwerx, J. (2020). NAD(+) homeostasis in health and disease. *Nat Metab*, *2*(1), 9–31. https://doi.org/10.1038/s42255-019-0161-5

Kim, L.-J, Chalmers, T. J., Smith, G. C., Das, A., Poon, E. W. K., Wang, J, Tucker, S. P., Sinclair, D. A., Quek, L.-E., & Wu, L. E. (2020). Nicotinamide mononucleotide (NMN) deamidation by the gut microbiome and evidence for indirect upregulation of the NAD+ metabolome. *bioRxiv*. https://doi.org/10.1101/2020.09.10.289561

Kucharczyk, R., Zagulski, M., Rytka, J., & Herbert, C. J. (1998). The yeast gene YJR025c encodes a 3-hydroxyanthranilic acid dioxygenase and is involved in nicotinic acid biosynthesis. *FEBS Letters*, *424*(3), 127–130. https://doi.org/10.1016/S0014-5793(98)00153-7

Lima, S., Khristoforov, R., Momany, C., & Phillips, R. S. (2007). Crystal structure of Homo sapiens kynureninase. *Biochemistry*, *46*(10), 2735–2744. https://doi.org/10.1021/bi0616697

Liu, L., Su, X., Quinn, W. J., 3rd, Hui, S., Krukenberg, K., Frederick, D. W., Redpath, P., Zhan, L., Chellappa, K., White, E., Migaud, M., Mitchison, T. J., Baur, J. A., & Rabinowitz, J. D. (2018). Quantitative analysis of NAD synthesis-breakdown fluxes. *Cell Metabolism*, *27*(5), 1067–1080. https://doi.org/10.1016/j.cmet.2018.03.018

Momany, C., Levdikov, V., Blagova, L., Lima, S., & Phillips, R. S. (2004). Three-dimensional structure of kynureninase from *Pseudomonas fluorescens*. *Biochemistry*, *43*(5), 1193–1203. https://doi.org/10.1021/bi035744e

Panozzo, C., Nawara, M., Suski, C., Kucharczyka, R., Skoneczny, M., Bécam, A. M., Rytka, J., & Herbert, C. J. (2002). Aerobic and anaerobic NAD+ metabolism in *Saccharomyces cerevisiae*. *FEBS Letters*, *517*(1-3), 97–102. https://doi.org/10.1016/s0014-5793(02)02585-1

Phillips, R. S. (2011). Structure, mechanism, and substrate specificity of kynureninase. *Biochimica et Biophysica Acta*, *1814*(11), 1481–1488. https://doi.org/10.1016/j.bbapap.2010.12.003

Pidugu, L. S., Neu, H., Wong, T. L., Pozharski, E., Molloy, J. L., Michel, S. L., & Toth, E. A. (2017). Crystal structures of human 3-hydroxyanthranilate 3,4-dioxygenase with native and non-native metals bound in the active site. *Acta Crystallographica. Section D, Structural Biology*, *73*(Pt 4), 340–348. https://doi.org/10.1107/S2059798317002029

Rajman, L., Chwalek, K., & Sinclair, D. A. (2018). Therapeutic potential of NAD-boosting molecules: The in vivo evidence. *Cell Metabolism*, *27*(3), 529–547. https://doi.org/10.1016/j.cmet.2018.02.011

Rentzsch, P., Witten, D., Cooper, G. M., Shendure, J., & Kircher, M. (2018). CADD: Predicting the deleteriousness of variants throughout the human genome. *Nucleic Acids Research*, *47*, 886. https://doi.org/10.1093/nar/gky1016

Shats, I., Williams, J. G., Liu, J., Makarov, M. V., Wu, X., Lih, F. B., Deterding, L. J., Lim, C., Xu, X., Randall, T. A., Lee, E., Li, W., Fan, W., Li, J. L., Sokolsky, M., Kabanov, A. V., Li, L., Migaud, M. E., Locasale, J. W., & Li, X. (2020). Bacteria boost mammalian host NAD metabolism by engaging the deamidated biosynthesis pathway. *Cell Metabolism*, *31*(3), 564–579. https://doi.org/10.1016/j.cmet.2020.02.001

Shi, H., Enriquez, A., Rapadas, M., Martin, E., Wang, R., Moreau, J., Lim, C. K., Szot, J. O., Ip, E., Hughes, J. N., Sugimoto, K., Humphreys, D. T., McInerney-Leo, A. M., Leo, P. J., Maghzal, G. J., Halliday, J., Smith, J., Colley, A., Mark, P. R., … Dunwoodie, S. L. (2017). NAD deficiency, congenital malformations, and niacin supplementation. *New England Journal of Medicine*, *377*(6), 544–552. https://doi.org/10.1056/NEJMoa1616361

Stevenson, R. E., & Hunter, A. G. (2013). Considering the embryopathogenesis of VACTERL Association. *Molecular Syndromology*, *4*(1–2), 7–15. https://doi.org/10.1159/000346192

Szot, J. O., Campagnolo, C., Cao, Y., Iyer, K. R., Cuny, H., Drysdale, T., Flores-Daboub, J. A., Bi, W., Westerfield, L., Liu, P., Leung, T. N., Choy, K. W., Chapman, G., Xiao, R., Siu, V. M., & Dunwoodie, S. L. (2020). Bi-allelic mutations in NADSYN1 Cause multiple organ defects and expand the genotypic spectrum of congenital NAD deficiency disorders. *American Journal of Human Genetics*, *106*(1), 129–136. https://doi.org/10.1016/j.ajhg.2019.12.006

Teste, M. A., Duquenne, M., Francois, J. M., & Parrou, J. L. (2009). Validation of reference genes for quantitative expression analysis by real-time RT-PCR in *Saccharomyces cerevisiae*. *BMC Molecular Biology*, *10*(1), 99. https://doi.org/10.1186/1471-2199-10-99

Trammell, S. A., Schmidt, M. S., Weidemann, B. J., Redpath, P., Jaksch, F., Dellinger, R. W., Li, Z., Abel, E. D., Migaud, M. E., & Brenner, C. (2016). Nicotinamide riboside is uniquely and orally bioavailable in mice and humans. *Nature Communications*, *7*, 12948. https://doi.org/10.1038/ncomms12948

Wentzel, C., Fernstrom, M., Ohrner, Y., Anneren, G., & Thuresson, A. C. (2008). Clinical variability of the 22q11.2 duplication syndrome. *European Journal of Medical Genetics*, *51*(6), 501–510. https://doi.org/10.1016/j.ejmg.2008.07.005

Winzeler, E. A., Shoemaker, D. D., Astromoff, A., Liang, H., Anderson, K., Andre, B., Bangham, R., Benito, R., Boeke, J. D., Bussey, H., Chu, A. M., Connelly, C., Davis, K., Dietrich, F., Dow, S. W., El Bakkoury, M., Foury, F., Friend, S. H., Gentalen, E., … Davis, R. W. (1999). Functional characterization of the S. cerevisiae genome by gene deletion and parallel analysis. *Science*, *285*(5429), 901–906. https://doi.org/10.1126/science.285.5429.901

Yang, Y., Liu, F., & Liu, A. (2018). Adapting to oxygen: 3-Hydroxyanthrinilate 3,4-dioxygenase employs loop dynamics to

accommodate two substrates with disparate polarities. *Journal of Biological Chemistry*, *293*(27), 10415–10424. https://doi.org/10.1074/jbc.RA118.002698

Zhang, Y., Colabroy, K. L., Begley, T. P., & Ealick, S. E. (2005). Structural studies on 3-hydroxyanthranilate-3,4-dioxygenase: the catalytic mechanism of a complex oxidation involved in NAD biosynthesis. *Biochemistry*, *44*(21), 7632–7643. https://doi.org/10.1021/bi047353l

SUPPORTING INFORMATION

Additional Supporting Information may be found online in the supporting information tab for this article.

How to cite this article: Szot, J. O., Slavotinek, A., Chong, K., Brandau, O., Nezarati, M., Cueto-González, A. M., Patel, M. S., Devine, W. P., Rego, S., Acyinena, A. P., Shannon, P., Myles-Reid, D., Blaser, S., Mieghem, T. V., Yavuz-Kienle, H., Skladny, H., Miller, K., Riera, M. D. T., Martínez, S. A., The CAUSES Study… Dunwoodie, S. L. (2021). New cases that expand the genotypic and phenotypic spectrum of Congenital NAD Deficiency Disorder. *Human Mutation*, 42, 862–876. https://doi.org/10.1002/humu.24211